Assessment of the potential iridology for diagnosing kidney disease using wavelet analysis and neural networks

Article *in* Biomedical Signal Processing and Control · November 2013

DOI: 10.1016/j.bspc.2013.04.006

CITATIONS
13

READS
31,996

3 authors, including:

Sherif Hussein
Mansoura University
19 PUBLICATIONS **101** CITATIONS

SEE PROFILE

Malcolm Granat
University of Salford
174 PUBLICATIONS **5,019** CITATIONS

SEE PROFILE

Biomedical Signal Processing and Control 8 (2013) 534–541

Contents lists available at SciVerse ScienceDirect

Biomedical Signal Processing and Control

journal homepage: www.elsevier.com/locate/bspc

Short communication

Assessment of the potential iridology for diagnosing kidney disease using wavelet analysis and neural networks

Sherif E. Hussein[a,*], Osama A. Hassan[b], Malcolm H. Granat[c]

[a] Computer and Systems Department, Mansoura University, Egypt
[b] International Medical Center, Cairo, Egypt
[c] University of Salford, Manchester, UK

ARTICLE INFO

Article history:
Received 4 December 2012
Received in revised form 19 April 2013
Accepted 24 April 2013

Keywords:
Complementary medicine
Iridology
Pervasive healthcare
Image processing
Wavelet analysis
Chronic renal failure

ABSTRACT

Alternative or complementary medicine emphasizes therapies that are claimed to improve quality of life, prevent disease, and address conditions that conventional medicine has limited success in curing. There are many techniques which are prevalent in many countries and these can cause harm if not scientifically evaluated. The objective of this paper is to validate the use of iridology to diagnose kidney abnormalities. Two subject groups were evaluated: one was 168 subjects free from kidney disease and the other was 172 subjects with chronic renal failure. The procedure to acquire, process and classify the iris images was designed in such a way that avoids any dependency on the iridologists by using wavelet analysis and Adaptive Neuro-Fuzzy Inference System. The results show a correct classification for both subjects with kidney problems and normal subjects of 82% and 93%, respectively. The proposed technique conducted on a systemic disease with ocular manifestations showed encouraging results. However, it is necessary to perform extensive studies with diseases that do not have ocular manifestations according to conventional medicine in order to validate iridology as a valid scientific technique.

1. Introduction

Complementary medicine is those therapies that are claimed to improve quality of life, prevent disease, and address conditions that conventional medicine has had limited success in curing, such as chronic back pain and certain cancers. Proponents of complementary medicine believe that these approaches to healing are safer and more natural and have been shown through experience to work. In certain countries, complementary medical practices are widely used methods of health care. However, many practitioners of modern conventional medicine believe these practices are unorthodox and unproven [1].

Although some medical schools have now begun offering complementary medicine, no standardized curriculum for medical students is available and there is still a debate about whether it should be offered at all. There is an argument that its inclusion in medical schools could be seen as an endorsement by conventional medicine, however if conventional medicine ignores it that will put patients at risk as complementary medicine use is so prevalent [2].

Complementary medicine regulation is a complicated and contentious issue. Currently only osteopaths and chiropractors have achieved statutory regulation in the UK. Theoretically anybody, regardless of insurance, skills or specialist knowledge, could set themselves up as a therapist. This leaves many clients with very little redress should they have a complaint. The UK government has been consulting on complementary medicine regulation since 2000 but progress has been slow. The main problem is achieving a consensus of the numerous therapy-specific regulatory organizations that already exist [3].

Iridology is a form of complementary medicine whose proponents believe patterns, colors, and other characteristics of the iris can be examined to determine information about a patient's systemic health. Practitioners match their observations to iris charts which divide the iris into zones corresponding to specific parts of the human body [4].

Peczely [5] and Liljequist [6] have independently noticed irises changes that correlate to different illnesses. They depicted in their publications very similar iris charts based on their own observations. Lane [7] carried out further surgical and autopsy correlations with iris markings which sparked the effort of Kritzer [8] and Jensen [4] to develop an updated iris charts that are widely used among iridologists as shown in Fig. 1. Typical charts divide the iris into approximately 80–90 zones. For example, the zone corresponding to the kidney is in the lower part of the iris, just beside 6 o'clock.

* Corresponding author. Tel.: +20 1060553903.
E-mail addresses: sherif_hussein@mans.edu.eg (S.E. Hussein), m.h.granat@salford.ac.uk (M.H. Granat).

1746-8094/$ – see front matter © 2013 Elsevier Ltd. All rights reserved.
http://dx.doi.org/10.1016/j.bspc.2013.04.006

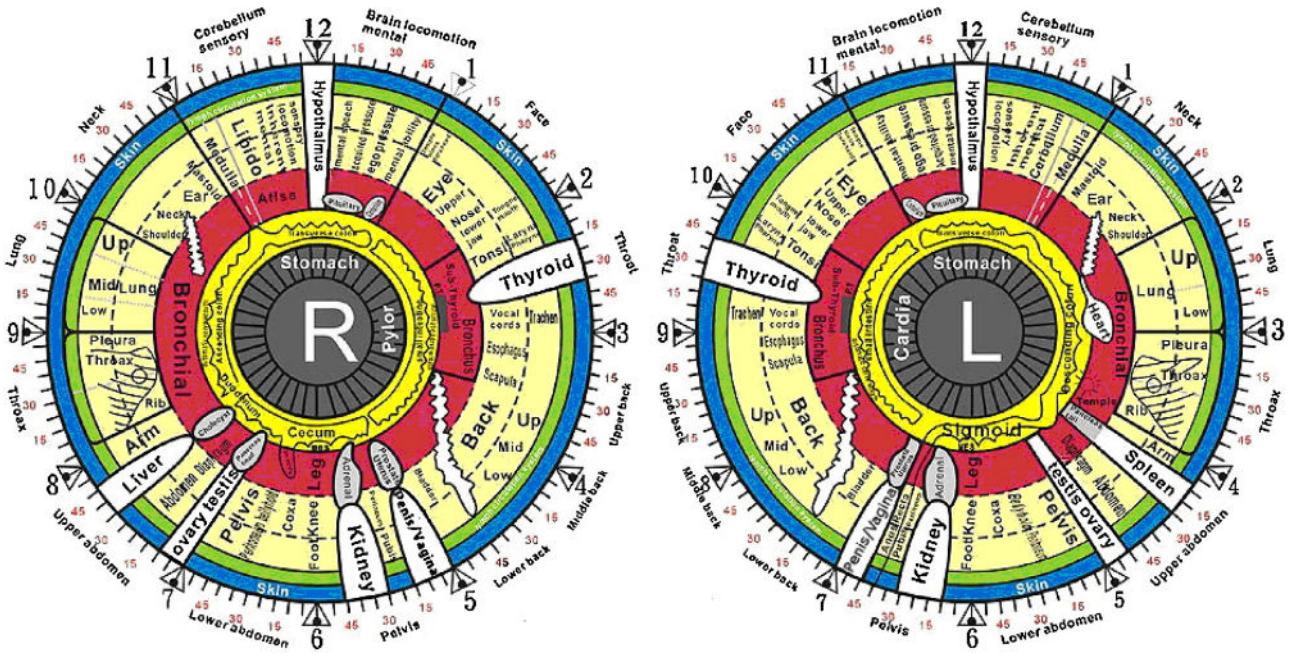

Fig. 1. The iridology chart for both the right and left irises.

However, there are minor variations between charts' associations of body parts and areas of the iris [9].

In an attempt to evaluate the diagnostic validity of iridology, many investigations have been conducted without a control group, and some (with or without a control group) were not evaluator blinded [10]. All of the uncontrolled studies and several of the unblinded experiments suggested that iridology was a valid diagnostic tool [11].

A number of researchers used blinded evaluations of the diagnostic validity of iridology. Simon et al. [12] studied patients suffering from kidney disease as defined by a creatinine level, and compared these to controls who were free of kidney disease. Photographs were taken of both irises of all 146 study participants, coded, and shown to 3 experienced iridologists and 3 ophthalmologists. The resulting frequency of false-positive and false-negative diagnoses was not significantly different from that expected by chance. Knipschild [13] conducted another investigator-masked case–control study. His 39 patients had inflamed gallbladder disease as confirmed by subsequent surgery. Patients with jaundice were excluded. Controls were matched for age and sex and had no signs or symptoms of gallbladder disease and shown to the iridologists. Validity, sensitivity, specificity, and consistency were not significantly different from that expected by pure chance.

Despite the lack of evidence for iridology, it is important to note that conventional medicine does not ignore the eyes as indicators of disease. There is a wide spectrum of systemic diseases that correlates with eye changes (the iris, the sclera, and the conjunctiva) [9]. For example, jaundice can indicate liver disease, dilated pupils can indicate brain malfunction, and even rings around the iris can indicate Wilson's disease (an abnormality of copper metabolism). Advanced kidney disease induces eye findings that signal the need for initiation or intensification of therapy. Conjunctival erythema, termed the red eyes of uremia, may be noted when high plasma phosphate levels induce corneal and conjunctival precipitation of calcium pyrophosphate. Metastatic calcification in the eyes may be associated with elevations of the serum concentration of calcium or calcium-phosphate product [14]. Profound uremia may rarely be complicated by transient cortical blindness; this is termed uremic amaurosis, which occurs in association with preserved pupillary contraction on light exposure and normal fundoscopic findings [15].

Some researchers have used iridology along with systematic and computerized approaches in medical applications. Ramlee and Ranjit used existing biometric identification methods to detect the presence of cholesterol in blood vessels. Based on the iris recognition methods, an iridology chart has been created to detect the presence of cholesterol in human body, however they did not evaluate their technique with a controlled study [16]. Shen et al. introduced the lacunae detection in iris images. As lacunae usually have poor local contrast, and the application of existing edge detection algorithms yields results which are not satisfactory, they proposed a lacunae detecting approach based on Gaussian filters that is robust to noise. The Gaussian filter in the vertical orientation was implemented to normalize iris image to reduce time complexity and again they failed to assess their findings with a controlled study or clarify how iridology was part of their technique [17].

Iridology, if proven correct, motivates healthy behavior and disease prevention throughout all stages of life which agrees with the objectives of pervasive healthcare technologies to offer new opportunities beyond traditional disease treatment that may play a major role in prevention. As indicated by Arnrich et al. [18], it was discussed the variability of health indicators between individuals and the manner in which relevant health indicators are provided to the users in order to maximize their motivation to mitigate or prevent unhealthy behaviors. From that perspective, iridology can pave the way for a pervasive, user-centered and preventive healthcare model. In this study, we evaluate the validity of iridology as a diagnostic tool. The case study in this research used iridology to detect abnormalities of the kidneys (chronic renal failure). We developed an automated technique based on image acquisition for the iris, pre-processing, normalization, segmentation, and feature extraction in regions corresponding to the kidneys in the iridology chart using the principles of iridology. The classification was based on those features and on the medical conditions of the patient.

2. Methodology

It has long been recognized that there is a lack of standardized procedures used in iridology and this research tries to overcome

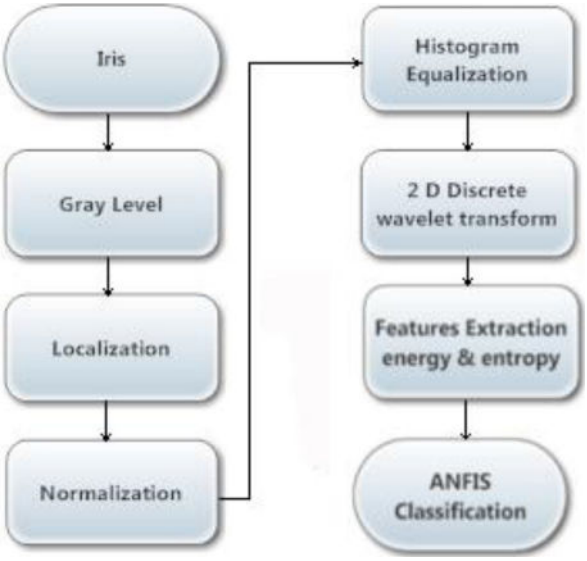

Fig. 2. Flow chart of diagnosing kidney disease using wavelet analysis and neural networks.

some of the problems that hindered the recognition of iridology as a probable medical technique for diagnosis. That technique, if proven correct, can accompany the conventional medical methods to screen the medical condition and assess the treatment progress. The protocol adopted in this research starts with subjects' selection, iris image acquisition, iris image processing to improve the required features, extracting the iris features and ending with classifying those features. The protocol is summarized in Fig. 2 and explained as follows:

2.1. Subjects selection and image acquisition

Chronic kidney disease (CKD) is a worldwide public health problem. It is recognized as a common condition that is associated with an increased risk of cardiovascular disease and chronic renal failure (CRF). The Kidney Disease Outcomes Quality Initiative (K/DOQI) of the National Kidney Foundation (NKF) defines chronic kidney disease as either kidney damage or a decreased glomerular filtration rate (GFR) of less than 60 mL/min/1.73 m^2 for 3 or more months. Whatever the underlying etiology, the destruction of renal mass with irreversible sclerosis and loss of nephrons leads to a progressive decline in GFR. The different stages of chronic kidney disease form a continuum in time.

According to K/DOQI, the classification of the stages of chronic kidney disease is as follows:

- Stage 1: Kidney damage with normal or increased GFR (>90 mL/min/1.73 m^2)
- Stage 2: Mild reduction in GFR (60–89 mL/min/1.73 m^2)
- Stage 3: Moderate reduction in GFR (30–59 mL/min/1.73 m^2)
- Stage 4: Severe reduction in GFR (15–29 mL/min/1.73 m^2)
- Stage 5: Kidney failure (GFR < 15 mL/min/1.73 m^2 or dialysis)

In stages 1 and 2 chronic kidney disease, GFR alone does not clinch the diagnosis. Other markers of kidney damage, including abnormalities in the composition of blood or urine or abnormalities on imaging studies, should also be present in establishing a diagnosis of stages 1 and 2 chronic kidney disease.

The K/DOQI definition and classification of chronic kidney disease allow better communication among physicians and facilitate intervention at the different stages. Patients with chronic kidney disease stages 1–3 are generally asymptomatic; clinical manifestations typically appear in stages 4–5. In this research, patients were chosen that are classified under stages 4 and 5 according to their GFR accompanied by blood and urine composition analysis without a priori information about their etiology. Some conditions can coexist with chronic kidney disease, as patients with chronic renal failure usually develop secondary hyperplasia of the parathyroid glands, resulting in elevated blood levels of parathyroid hormone (PTH). Those coexisting conditions however were not taken into account as the focus was on the presence or absence of chronic renal failure. Subjects with healthy kidneys were assessed using the same screening method while preliminary eye checks were not part of this screening method.

A pool of 213 patients, who had chronic kidney disease, were investigated after their informed consent and only 172 of them had chronic renal failure with stage 4 or 5 (GFR $\leq$ 29). One hundred sixty eight normal subjects with healthy kidney condition were selected as controls. The mean age values of the patients with chronic renal failure and the subjects in the group with healthy kidneys were 56 and 52 years, respectively, as shown in Table 1.

In this research, a MultiPIX Handheld Iridology Camera, Iris Supplies Ltd., was used to capture the eye image [19]. The choice of this portable camera with a lighting system that includes; dual fiber-optic side lighting for better iris fiber definition, variable intensity adjustment, single (medial and lateral) to twin lighting, cold-light minimizing patient irritation, and precise daylight illumination for optimum exposure. That leads to the ability to eliminate any artifacts or illumination variation.

2.2. Image processing

The research protocol needs to separate the iris from both the pupil and the sclera and then normalize the iris to a standard dimension that can be matched with the iris charts. The protocol needs to have the capability of feature extraction and a classification mechanism to infer the right diagnosis.

To realize the processing needed for detecting the iris center and the pupil center, the color image was transformed from color image into a gray level image then segmented and transformed to polar coordinates.

2.2.1. Iris localization

Iris localization is used to locate the inner and outer boundaries of an iris. The inner boundary can be found by detecting a pupil area where its perimeter designates the inner boundary of the iris. The iris outer boundary is a circular edge separating the iris from the sclera zone. Iris edge detection is the locating of points on the inner and outer boundary of iris. The average gray value of the pupil is the minimum and that of sclera is the maximum, and the average value of iris is between them. Therefore, on the iris inner and outer boundaries the edge intensity of a pixel must be a maximum. Both boundaries can be located by using intensity differences among parts of the eye (pupil, iris, and sclera) and circular shape of the pupil and iris (Fig. 3).

The technique used in this research is the Hough transform. It is a standard computer vision algorithm that can be used to determine the parameters of simple geometric objects, such as lines and circles, present in an image. The circular Hough transform can be employed to deduce the radius and center coordinates of the pupil and iris regions. An automatic segmentation algorithm based on the circular Hough transform is employed by Wildes et al. [20], Kong and Zhang [21], Tisse et al. [22], and Ma et al. [23]. Firstly, an edge map is generated by calculating the first derivatives of intensity values in an eye image and then thresholding the result. From the edge map, votes are cast in Hough space for the parameters of circles passing through each edge point. These parameters are the

Table 1
Patients with chronic renal failure and subjects with healthy kidney age and gender.

	Mean age	Age standard deviation	Number of males	Number of females	Total number
Patients with chronic renal failure	56	3.7	96	76	172
Subjects with healthy kidney	52	5.3	88	80	168

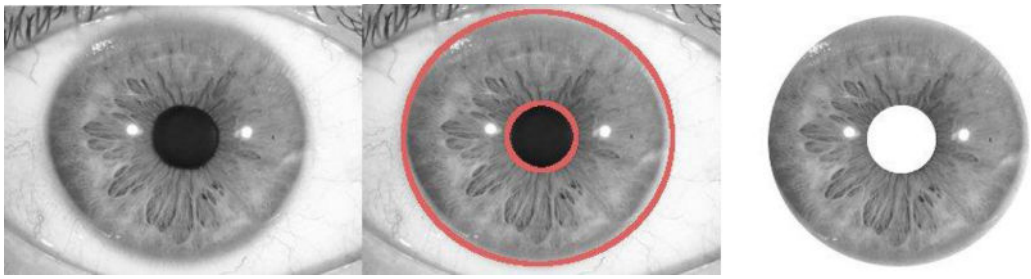

Fig. 3. Stages of iris localization. Left, greyscale eye image. Middle, two circles overlayed for iris and pupil boundaries in red color. Right, the segmented iris. (For interpretation of the references to color in text, the reader is referred to the web version of this article.)

center coordinates x_c and y_c, and the radius r, which are able to define any circle according to the equation

$$x_c^2 + y_c^2 - r^2 = 0 \quad (1)$$

A maximum point in the Hough space will correspond to the radius and center coordinates of the circle best defined by the edge points.

2.2.2. Transformation from Cartesian to polar coordinates

Robust representations for the iris must be invariant to changes in the size, position and orientation of the patterns. Irises from different people may be captured in different sizes and, even for irises from the same eye; the size may change due to illumination variations and other factors. In order to compensate the varying size of the captured iris, it is common to translate the segmented iris region, represented in the Cartesian coordinate system, to a fixed length and dimensionless polar coordinate system as shown in Fig. 4.

The technique used in this research is the homogenous rubber sheet model devised by Daugman [24] which remaps each point within the iris region to a pair of polar coordinates (r, θ) where r is on the interval [0,1] and θ is angle $[0,2\pi]$.

The remapping of the iris region from (x,y) Cartesian coordinates to the normalized non-concentric polar representation is modeled as

$$I(x(r,\theta), y(r,\theta)) \rightarrow I(r,\theta) \quad (2)$$

with

$$x(r,\theta) = (1-r)x_p(\theta) + rx_l(\theta) \quad (3)$$

$$y(r,\theta) = (1-r)y_p(\theta) + ry_l(\theta) \quad (4)$$

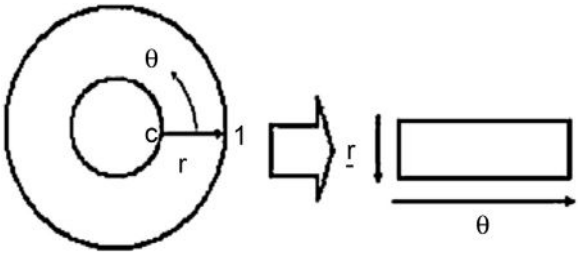

Fig. 4. Transformation of the iris from Cartesian coordinates to polar coordinates.

where $I(x,y)$ is the iris region image, (x,y) are the original Cartesian coordinates, (r,θ) are the corresponding normalized polar coordinates, and x_p, y_p and x_l, y_p are the coordinates of the pupil and iris boundaries along the θ direction. The rubber sheet model takes into account pupil dilation and size inconsistencies in order to produce a normalized representation with constant dimensions. In this way the iris region is modeled as a flexible rubber sheet anchored at the iris boundary with the pupil center as the reference point.

It is worth mentioning here that even though the homogenous rubber sheet model accounts for pupil dilation, imaging distance and non-concentric pupil displacement, it does not compensate for rotational inconsistencies which can shift the iris regions in the θ direction. To compensate for those possible inconsistencies, the subject's eyes needed to be aligned horizontally during the image acquisition stage in the experimental procedure.

2.2.3. Histogram equalization

To improve the iris image contrast, a stage of histogram equalization was needed. In the histogram of the normalized iris, gray levels are concentrated at the center of gray level from 0 to 255. To perform histogram equalization, we have to calculate the probability density function and the cumulative density function of the image. This involves counting the number of pixels of each color in the image, and producing a running sum of the count. Then by simply scaling the output, we could perform histogram equalization. An iris, whose pixels tend to occupy the entire range of possible gray levels and, in addition, tend to be distributed uniformly, will have an appearance of high contrast and will exhibit a large variety of gray tones [25] as shown in Fig. 5.

2.3. Features extraction

Wavelet transforms are finding intense use in fields as diverse as telecommunications and biology. Because of their suitability for analyzing non-stationary signals, they have become a powerful alternative to Fourier methods in many medical applications, where such signals abound [26]. The wavelet transform, being a linear operation, does not produce interference terms. Unlike the Fourier transform, it possesses a capability of time–space localization of signal spectral features. For these reasons, much interest in applications of the wavelet transform to texture analysis can be noticed recently [27].

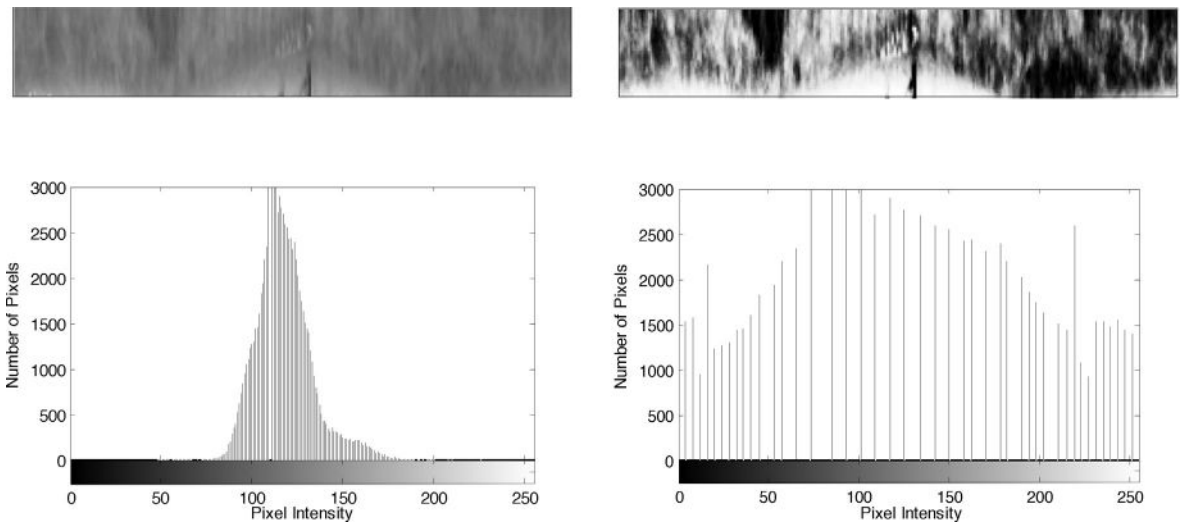

Fig. 5. The iris histogram equalization. Top left, original iris image. Bottom left, original iris image histogram. Top right, the histogram equalized iris image. Bottom right, its histogram.

The continuous wavelet transform of a 1-D signal $f(x)$ is defined as:

$$(W_\psi f)(a,b) = \langle f, \psi(a,b)\rangle = \int_{-\infty}^{+\infty} f(x)\psi^*_{(a,b)}(x)dx \quad (5)$$

$$\psi_{(a,b)} = a^{-1/2}\psi\left(\frac{x-b}{a}\right) \quad (6)$$

where a is the scaling factor, b is the translation parameter related to the location of the window, and $\psi^*(x)$ is the transforming function. The extension to 2-D is usually performed by using a product of 1-D filters. The transform is computed by applying a filter bank to the image. The rows and columns of an image are processed separately and down sampled by a factor of 2 in each direction, resulting in one low pass image LL and three detail images HL, LH, and HH. The LH channel contains image information of low horizontal frequency and high vertical frequency, the HL channel contains high horizontal frequency and low vertical frequency, and the HH channel contains high horizontal and high vertical frequencies. Note that in multi-scale wavelet decomposition, only the LL sub band is successively decomposed.

Wavelets can be used to decompose the data in the iris region into components that appear at different resolutions. Wavelets have the advantage over traditional Fourier transform in that the frequency data are localized, allowing features which occur at the same position and resolution to be matched up. A number of wavelet filters, also called a bank of wavelets, are applied to the 2D iris region, one for each resolution with each wavelet a scaled version of some basis function. The output of applying the wavelets is then evaluated to extract iris features that correspond to the kidney's condition.

2.3.1. Gabor filtering

The Gabor function has the property of finite effective width in both the spatial and spectral domains. The property is relevant to texture analysis, especially texture segmentation since different textures tend to concentrate, in many cases, their significant energies into certain narrow frequency ranges. It consists in convolution of image with complex Gabor filters. As a product of this operation, complex coefficients are computed with one-level decomposition [28].

The feature of the iris texture combines the position information and orientation information. The normalized iris images are divided into blocks. The Gabor filter is used to extract iris feature from the block that correspond to the kidney.

To extract the features necessary for texture classification from the iris zone that represents the kidney (that corresponds to both the right and left eyes as shown in Fig. 6), the methodology has been divided into two layers; these are the wavelet decomposition layer and the entropy and energy calculation layer.

(1) Wavelet decomposition layer: for wavelet decomposition of each iris zone, the pyramid wavelet structure is used. We obtain one-level wavelet decomposition, and save the four images where H and L stand for the high pass and low pass band in each of the horizontal and vertical orientations for the subsequent calculation of entropy and energy quantities.
(2) Entropy and energy calculation layer: this layer is responsible for calculating the entropy and energy quantities of each image. Thus, entropy and the energy quantities are the features that characterize the four images giving a total of 8 features for each iris.

2.3.2. Entropy

Entropy is a quantity that is widely used in information theory and is based on probability theory [29]. Entropy is a common concept in many fields, mainly in mechanics, image processing, and signal processing. The general form of the entropy is given by:

$$H(X) = -\sum_{i=1}^{n} p_i \log_2 p_i \quad (7)$$

where X is a random variable which can be one of the values x_1, x_2, ..., x_n with probabilities p_1, p_2, ..., p_n. Note that if $p_i = o$, then

Fig. 6. The right and left irises in polar coordinates and the blocks that corresponds to the kidney in each iris.

$0 \log_2 0$ is defined as 0. Thus, $H(X)$ can be interpreted as representing the amount of uncertainty that exists in the value of X. In information theory, entropy value is considered to be an average amount of information received when the value of X is observed. In this paper, we use the norm entropy. The norm entropy H is defined as follows:

$$H_{B,l}^{X_m} = \sum_{i=0}^{N}\sum_{j=0}^{N} \left| w_{B,l,i,j}^{X_m} \right|^p, \quad \text{for} (1 \le p < 2) \tag{8}$$

where $w_{B,l,i,j}^{X_m}$ is the wavelet coefficient at (i,j) location at l scale in B ($B \in \{\text{LH, HL, HH}\}$) sub band and X_m is the color space ($m = 1, 2, 3$) [30,31].

2.3.3. Energy

Energy is commonly used for texture analysis. In this study, we use the averaged l2-norm, which is defined as follows:

$$E_{B,l}^{X_m} = \frac{1}{N \times N} \sum_{i=0}^{N}\sum_{j=0}^{N} \left(w_{B,l,i,j}^{X_m} \right)^2 \tag{9}$$

where $w_{B,l,i,j}^{X_m}$ is the wavelet coefficient at (i,j) location at l scale in B ($B \in \{\text{LH, HL, HH}\}$) sub band and X_m is the color space ($m = 1, 2, 3$) [30].

2.4. Classification and diagnosis

The proposed method uses Adaptive Neuro-Fuzzy Inference System (ANFIS) for classification of features from both chronic renal failure and normal groups. It is considered a robust technique, since ANFIS is an approach that is able to handle the uncertainty present in the system. It combines a NN and a fuzzy system together to offer a classification capability superior or comparable to artificial neural network, classification and regression tree, logistic regression, and support vector machine [32,33].

ANFIS is functionally based on the Surgeno-type fuzzy rule base and at the same time has an architecture equivalent under some constraints [27] to a radial basis function neural network, allowing the system to learn from the training data. The design started by subtractive clustering to determine the number of rules and the input membership functions. The membership function of choice was the generalized bell function:

$$\mu(x) = \frac{1}{1 + \left| x - c/a \right|^{2b}} \tag{10}$$

where the parameters a and b vary the width of the curve and the parameter c locates the center of the curve. The parameter b should be positive.

Subtractive clustering is an unsupervised algorithm based on a measure of the density of the normalized data points in the feature space. The point with the highest number of neighbors is selected as the center for a cluster. The data points within a pre-specified fuzzy radius are then removed and the algorithm looks for a new point with the highest number of neighbors until all the data points are checked. The following two rules were a part of the first-order Surgeno-type rule base:

If u_1 is A_1 and u_2 is B_1, then

$$y_1 = c_{11}u_1 = c_{12}u_2 = c_{10} \tag{11}$$

If u_1 is A_2 and u_2 is B_2, then

$$y_2 = c_{21}u_1 + c_{22}u_2 + c_{20} \tag{12}$$

The fuzzy classifier can interpolate between the two linear rules depending on their state. So, if the firing strengths of the rules are α_1 and α_2 for two inputs u_1 and u_2, respectively, then the output based on weighted average is:

$$y = \frac{\alpha_1 y_1 + \alpha_2 y_2}{\alpha_1 + \alpha_2} \tag{13}$$

$$\begin{aligned} y = {} & \beta_1 y_1 + \beta_2 y_2 = \beta_1(c_{11}u_1 + c_{12}u_2 + c_{10}) \\ & + \beta_2(c_{21}u_1 + c_{22}u_2 + c_{20}) = \beta_1 c_{11}u_1 + \beta_1 c_{12}u_2 + \beta_1 c_{10} \\ & + \beta_2 c_{21}u_1 + \beta_2 c_{22}u_2 + \beta_2 c_{20} \end{aligned} \tag{14}$$

Using the least-squares method, c_{ij} ($i = 1, 2$ and $j = 0, 1, 2$) could be adjusted in the forward pass while the membership function's parameters a_i, b_i, and c_i could be adjusted by gradient descent using the error signals that propagate in the backward pass [34].

3. Results

A database of RGB color iris images was constructed representing two images for each iris for both chronic renal failure group and healthy kidney group which add up to 680 pairs of images for both right and left iris. Every two pairs of subject's images are kept together and randomly arranged in their corresponding group of subjects. Those images are transformed to gray levels based on luminosity. The database images undertook another stage of transformation to be segmented and mapped to polar coordinates with a fixed size of 80×720 pixels for each image. The zones that corresponds to the kidney on the iris maps were then selected from the data base to be of size 40×24 pixels from point (40, 549) to point (80, 573) for the right iris and from point (40, 507) to point (80, 531) for the left iris. For each of those images, Discrete Gabor Transform was calculated with one-level decomposition to produce 4 sub images. The transformation is subsequently fed to an entropy and energy calculation layer to produce 8 features for each iris.

For the training data, the first 232 pairs of images were selected which formed 232×8 right iris features from subjects with chronic renal failure and the first 216 pairs of images were selected which formed 216×8 right iris features from subjects with healthy kidney and were then used in the learning stage of the neural network that corresponds to right iris. While the same number of features from same pairs but from left iris were used in the learning stage for the neural network that corresponds to left iris.

Using these sets of features, a neuro-fuzzy classifier was then designed to classify the subject into either the chronic renal failure group or the healthy kidney group. The output was set to be one for each of the neural networks (right and left iris) if the subject has chronic renal failure and was set to be zero for subjects with healthy kidney. Training was done using 10-fold cross-validation in which learning data were randomly partitioned into 10 nearly equally sized folds. Subsequently 10 iterations of training and validation are performed such that, within each iteration a different fold of data is held-out for validation while remaining 9 folds are used for learning. Training was continued for 10,000 epochs for each run and the 10 results from the folds are averaged [35]. The neural network that corresponds to each iris with the least average cross-validation error was then selected. Five generalized bell membership functions for each of the eight inputs as well as a rule base of 67 rules were found with a training error of 0.152 for the designed right iris classifier. While five generalized bell membership functions and a rule base of 79 rules were found with a training error of 0.186 for the designed left iris classifier.

In the testing stage, the remaining of features 112×8 for subjects with chronic renal failure for both right and left iris and 120×8 for subjects with healthy kidney were used. Condition for success to produce a meaningful diagnosis was values equal to or less than 0.2 that represent healthy kidneys or values equal to or greater than

Table 2
Results.

	Kidney problems	Normal kidney
Number of tests	56	60
Correct classifications	46	56
False classification	3	1
No classification	7	3

0.8 that represent chronic renal failure, while values in between 0.2 and 0.8 were considered undetermined classification. In addition, if any of the right or left iris neural network gives a diagnosis of chronic renal failure that means an overall diagnosis of chronic renal failure. As there are two pairs of images for each subject, it is sufficient that only one of those two pairs is diagnosed as chronic renal failure. For healthy kidney diagnosis both eyes needs to have a normal outcome.

The results in Table 2 for the testing subjects (56 subjects with chronic renal failure and 60 subjects with healthy kidney) show a correct classification for both subjects with kidney problems and normal subjects of 82% and 93%, respectively. While false classifications for the both groups are 6% and 2%, respectively. On the other hand, no classification for subjects with kidney problems and normal subjects are 12% and 5%, respectively.

False negative classification is considered one of the most significant factors in the designed classifier performance which is found to be 6%. That percentage indicates that out of 100 subjects with chronic renal failure there are 6 subjects that could be misdiagnosed.

4. Discussion and conclusion

In this paper, Discrete 2-D Gabor Transform and ANFIS were applied to iris zones that correspond to the kidneys as claimed by the iridologists to classify the kidneys pathological conditions. The technique adopted in this research provides automated methods with artificial intelligence techniques to assess the correlation between the iris and the kidneys health. The classification technique used shares similarities to that used in the iris biometric identification technique which uses the unique epigenetic patterns of a human iris for personal identification. Biometric identification employs image processing and signal processing methods to extract information from the unique iris structure from a digitized image of an eye though coding the wavelet coefficients for the main iris texture. While the technique used here identifies the fine discrepancies that appear in the iris texture through energy and entropy for wavelet decomposition and without coding.

In addition, the different reasons that could hinder the proper diagnosis of the iridologists and consequently were the reason for losing faith in that technique had been identified. Those reasons were the lack of an automated methodology that not only based on properly diagnosed subjects but also on controlled studies.

In this research, the technique used was applied to the gray level of the picture taken from pre-diagnosed subjects as the classification was based on the iris texture.

It can be revealed from this research a few factors that can affect the correct classification. Firstly, there is the image processing methods which selectively improve the iris features. Secondly, the features selection optimally represents the correlation between the iris and the kidney pathology. Finally, there is the choice of zone/zones that represent the organ under investigation which we have taken according to the iridologists' charts. The results showed a false-negative and a false-positive diagnosis of 6% and 2%, respectively.

Despite these encouraging results, the proposed technique was conducted on a systemic disease with ocular manifestations. It is necessary to perform extensive studies with diseases that do not have ocular manifestations according to conventional medicine in order to validate iridology as a valid scientific technique and hence to be recognized in clinical practice for both screening and treatment assessment and open the way for pervasive healthcare.

References

[1] E. Ernest, Healing, Hype or Harm? Societas, 2008.
[2] J. Beder, Hospital Social Work: The Interface of Medicine and Caring, Routlege, New York, 2006.
[3] K. Boddy, B. Wider, M.H. Pittler, E. Ernst, Oxford Handbook of Complementary Medicine, Oxford University Press, USA, 2008, June.
[4] B. Jensen, Iridology Simplified, 5th ed., Iridologists International, California, USA, 1980.
[5] K. Hanns, M. Stöhr, Ärzte, Heiler, Scharlatane: Schulmedizin und Alternative Heilverfahren Auf Dem Prüfstand, Springer, 2002, ISBN 3798513058, pp. 183.
[6] N. Liljequist, The Diagnosis from the Eye, The Iridology Publishing Co., 1916.
[7] H.E. Lane, Diagnosis from the Eye, BiblioBazaar, 2008.
[8] D. Cline, H.W. Hofstetter, J.R. Griffin, Dictionary of Visual Science, 4th ed., Butterworth-Heinemann, Boston, 1997, ISBN 0-7506-9895-0.
[9] B. Jensen, Science and Practice of Iridology, Whitman Publications, 2005, May.
[10] V.V. Pokanevych, Iridology in Ukraine Lik Sprava 3 (1998) 152–156.
[11] K. Münstedt, S. El-Safadi, F. Brück, M. Zygmunt, A. Hackethal, H.R. Tinneberg, Can iridology detect susceptibility to cancer? A prospective case-controlled study, Journal of Alternative and Complementary Medicine 11 (2005) 515–519.
[12] A. Simon, D.M. Worthen, J.A. Mitas, An evaluation of iridology, Journal of American Medical Association 242 (1979) 1385–1387.
[13] P. Knipschild, Looking for gall bladder disease in the patient's iris, British Medical Journal 297 (1988) 1578–1581.
[14] C.H. Hsiao, A. Chao, S.Y. Chu, Association of severity of conjunctival and corneal calcification with all-cause 1-year mortality in maintenance haemodialysis patients, Nephrology, Dialysis, Transplantation 26 (2011) 1016.
[15] H.R. Tyler, Neurologic disorders seen in the uremic patient, Archives of Internal Medicine 126 (1970) 781.
[16] R.A. Ramlee, S. Ranjit, Using iris recognition algorithm, detecting cholesterol, in: 2009 International Conference on Information Management and Engineering, April, 2009, pp. 714–717.
[17] B. Shen, Y. Xu, G. Lu, D. Zhang, Detecting iris lacunae based on Gaussian filter, in: Third International Conference on International Information Hiding and Multimedia Signal Processing, November, 2007, pp. 233–236.
[18] B. Arnrich, O. Mayora, J. Bardram, G. Trıster, Pervasive Healthcare, Methods of Information in Medicine 49 (2010) 67–73, http://dx.doi.org/10.3414/ME09-02-0044.
[19] http://www.iris-supplies.com.au (accessed January 2013).
[20] R. Wildes, J. Asmuth, G. Green, S. Hsu, R. Kolczynski, J. Matey, S. McBride, A system for automated iris recognition, in: Proceedings of IEEE Workshop on Applications of Computer Vision, Sarasota, FL, 1994, pp. 121–128.
[21] W. Kong, D. Zhang, Accurate iris segmentation based on novel reflection and eyelash detection model, in: Proceedings of 2001 International Symposium on Intelligent Multimedia, Video and Speech Processing, Hong Kong, 2001.
[22] C. Tisse, L. Martin, L. Torres, M. Robert, Person identification technique using human iris recognition, in: International Conference on Vision Interface, Canada, 2002.
[23] L. Ma, Y. Wang, T. Tan, Iris Recognition Using Circular Symmetric Filters, National Laboratory of Pattern Recognition, Institute of Automation, Chinese Academy of Sciences, 2002.
[24] J. Daugman, High confidence visual recognition of persons by a test of statistical independence, IEEE Transactions on analysis and Machine Intelligence 15 (11) (1993, November) 1148–1161.
[25] C.M. Patil, S.P. Kulkarni, An approach of iris feature extraction for personal identification, in: 2009 International Conference on Advances in Recent Technologies in Communication and Computing, 2009, October, pp. 796–799.
[26] S. Mallat, A Wavelet Tour of Signal Processing, 3rd ed., Academic Press, 2008, December.
[27] A. Sengur, Wavelet transform and adaptive neuro-fuzzy inference system for color texture classification, Expert Systems with Applications 34 (3) (2008) 2120–2128.
[28] B.N. Lavanya, K.B. Raja, K. Venugopal, R.L.M. Patnaik, Minutiae extraction in fingerprint using Gabor filter enhancement, in: International Conference on Advances in Computing, Control, and Telecommunication Technologies, December, 2009, pp. 54–56.
[29] A. Sengur, I. Türkoğlu, M.C. ve İnce, Wavelet oscillator neural networks for texture segmentation, Neural Network World 4 (2008) 275–289.
[30] R.R. Coifman, M.V. Wickerhauser, Entropy-based algorithms for best basis selection, IEEE Transactions on Information Theory 38 (2) (1992) 713–718.
[31] U. Rajendra Acharya, F. Molinari, S. Vinitha Sree, S. Chattopadhyay, K.-H. Ng, J.S. Suri, Automated diagnosis of epileptic EEG using entropies, Biomedical Signal Processing and Control 7 (4) (2012, July) 401–408.

[32] K. Tanabe, B. Lucic, D. Amic, T. Kurita, M. Kaihara, N. Onodera, Prediction of carcinogenicity for diverse chemicals based on substructure grouping and SVM modeling, Molecular Diversity 14 (4) (2010) 789–802.
[33] C.D. Katsis, N.S. Katertsidis, D.I. Fotiadis, An integrated system based on physiological signals for the assessment of affective states in patients with anxiety disorders, Biomedical Signal Processing and Control 6 (3) (2011, July) 261–268.
[34] İ. Güller, E.D. Übeyli, Application of adaptive neuro-fuzzy inference system for detection of electrocardiographic changes in patients with partial epilepsy using feature extraction, Expert Systems with Applications 27 (3) (2004) 323–330.
[35] G.C. Cawley, N.L.C. Talbot, On over-fitting in model selection and subsequent selection bias in performance evaluation, Journal of Machine Learning Research (2010) 2079–2107.